J Nanopart Res (2011) 13:6591–6601
DOI 10.1007/s11051-011-0566-x

RESEARCH PAPER

Gold, silver, and palladium nanoparticle/nano-agglomerate generation, collection, and characterization

Sunita R. Boddu · Veera R. Gutti · Tushar K. Ghosh · Robert V. Tompson · Sudarshan K. Loyalka

Received: 24 August 2010 / Accepted: 29 August 2011 / Published online: 18 September 2011

Abstract Generation, collection, and characterization of gold, silver, and palladium nanoparticles and nano-agglomerates (collectively "nanoparticles") have been explored. The nanoparticles were generated with a spark aerosol generator (Palas GFG-1000). They were collected using a deposition cell under diffusion and thermophoresis. The shapes and sizes of the deposited particles were measured using transmission electron microscopy (TEM). TEM images showed that the particles were in the range of 8–100 nm in diameter, and their shapes varied from nearly spherical to highly non-spherical. Thermophoresis enhanced the deposition of nanoparticles (over the diffusive or the isothermal deposition) in all cases. Further, the size distributions of the nanoparticles generated in the gas phase (aerosol) were measured using a scanning mobility particle sizer (SMPS 3080, TSI) spectrometer. The SMPS results show that an increase in the spark frequency of the generator shifted the size distributions of the nanoparticles to larger diameters, and the total particle mass production rate increased linearly with increase in the spark frequency. The computational fluid dynamics code Fluent (Ansys) was used to model the flow in the deposition cell, and the computed results conform to the observations.

Keywords Nanoparticle · Nano-agglomerate · Spark generation · Deposition · Cancer treatment · Thermophoresis · Nanomedicine

S. R. Boddu · V. R. Gutti · T. K. Ghosh · R. V. Tompson · S. K. Loyalka (✉)
Nuclear Science & Engineering Institute and Particulate Systems Research Center, University of Missouri, E2433 Lafferre Hall, Columbia, MO 65211, USA
e-mail: LoyalkaS@missouri.edu

Introduction

In recent years, noble metal nanoparticles and their nano-sized agglomerates (collectively referred to as nanoparticles or particles in the subsequent sections) have been the subjects of much focused research due to their unique electronic, optical, mechanical, magnetic, and chemical properties that can be significantly different from those of bulk materials. To enhance their use, it is important to understand the generation, transport, deposition, and interaction of such particles. For example, the diffusive transport of gold nanoparticles in the design of therapeutic drugs for cancer treatment, and elucidation of the transport and deposition of particles in nuclear reactor containments and reactor cores for very high temperature reactor designs are two widely different applications with similar nanoparticle related needs.

There has been considerable interest recently in the synthesis and applications of gold (Cao 2004; Hsu 2004; Huang 2006; Frieboes et al. 2006; Kannan et al.

2006; Antonello and Bocci 2007; Pathak et al. 2007; De Jong et al. 2008), silver (Bae et al. 2002; Kumar et al. 2003; Zhang et al. 2004; Patel et al. 2005; Kim et al. 2005; Chaudhari et al. 2007; Pal et al. 2007; Chen and Gao 2007), and palladium (Jenson et al. 1980; Ache et al. 1989; Ozawa et al. 2002; Giridhar et al. 2006) nanoparticles. Since a number of issues remain, including control of sizes, shapes, and rates of production, it is of interest to explore further their generation and synthesis.

Our objective in this article is to report on the exploration of the generation, collection, and characterization of gold, silver, and palladium nanoparticles. Aerosol generation by spark discharge method is of special interest because it is continuous, clean, flexible with respect to material, and scale-up is possible (Evans et al. 2003; Lehtinen et al. 2004; Byeon et al. 2008; Tabrizi et al. 2009; Boddu et al. 2011). We used a spark aerosol generator (GFG-1000, Palas) to generate primary particles and a thermophoretic deposition cell for sample collection. Transmission electron microscopy (TEM) and scanning electron microscopy (SEM) were used to characterize the deposited particles. We also used a scanning mobility particle sizer (SMPS) spectrometer to measure the particle size distributions in the aerosol phase. The computational fluid dynamics (CFD) code Fluent (Ansys) was employed to compute the deposition mass fractions of nanoparticles in the deposition cell and to estimate the increase in particle deposition due to thermophoresis. We obtained experimental data for nanoparticle deposition at different spark frequencies that conform to the results based on the CFD modeling of the deposition efficiencies.

Experimental methods

Particle generation

The GFG-1000 spark aerosol generation system (Palas) consists of two electrodes, made of material of interest for generation of nanoparticles, separated by a 1.8 mm gap. One of the electrodes was connected to a high voltage (3,000 V) supply in parallel with a capacitor (20 nF). Charge stored in the capacitor is discharged at a set frequency which produces sparks across the electrode gap. Each electric spark locally evaporates the electrode material in the vicinity of the spark. The evaporated material (atoms/ions) nucleates to very fine primary particles in a controlled gaseous flow, and grows further via agglomeration and condensation. The particle production rate and sizes depend on the spark frequency, and the size/shape distributions are also affected by the gaseous environment and flow rate.

Particle collection

Nanoparticles have low inertia compared with larger particles and have low diffusivities compared with gaseous molecules. Thus, their collection by either inertial impaction or diffusional deposition processes alone is not very efficient. We have collected particles on TEM grids in thermal gradients utilizing thermophoresis for particle deposition. A schematic diagram of the experimental set up for particle generation and subsequent deposition on TEM grids in a deposition cell is shown in Fig. 1.

Argon gas exiting the particle generator is heated to a temperature of 100 °C as it passes through a cylindrical heating tube wrapped with a heating tape. When the exiting argon gas is observed to have reached a temperature of 100 °C, we initiate sparking between the two electrodes and particle generation begins. The particle/gas mixture then flows into the thermophoretic deposition cell. A carbon-coated copper TEM grid is placed on the notch shown in Fig. 1. The aluminum rod on which the notch (for positioning of a TEM grid) is located was cooled using an ice bath which results in an initial temperature at the notch of 7 °C. This temperature rises steadily during the particle collection interval to about 17 °C, depending on the gas flow rate.

A 3-way valve is positioned at the inlet of the thermophoretic deposition cell such that the heated particle/gas mixture enters the valve and exits to either the thermophoretic cell or to the atmosphere. This allows the heated, particle laden argon flow to be directed into the deposition cell as a step function, once the steady-state particle generation, heating of the flow, and cooling of the copper TEM grid are established. Particle collection times were fixed at 2 min for all experimental runs. The nanoparticles deposited on the TEM grids were studied using TEM, SEM, and energy dispersive X-ray spectroscopy (EDS). We deposited particles in the deposition cell under isothermal conditions as a control, i.e., when the argon gas and TEM

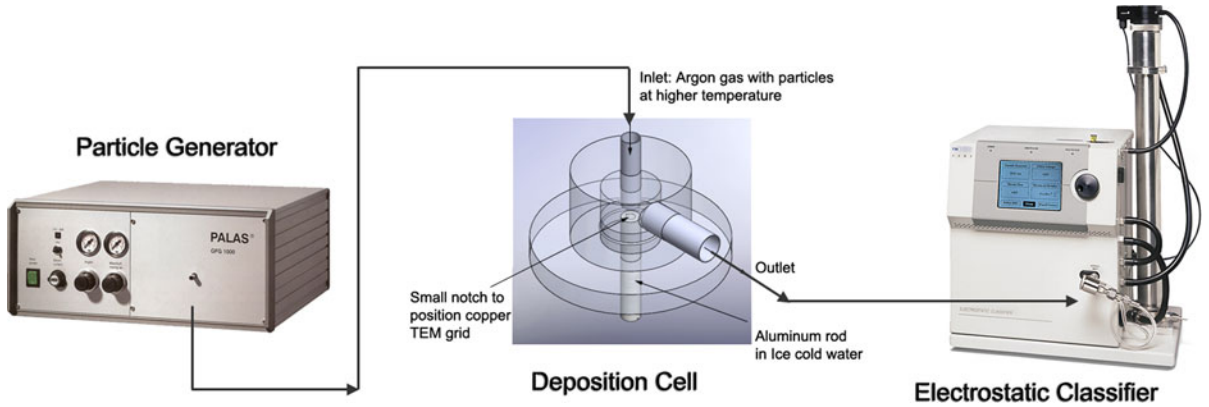

Fig. 1 A schematic diagram of the experimental set up for particle generation, deposition in thermophoretic cell, and electrostatic classifier for size distribution measurement

grid are kept at the ambient temperature, and convection and diffusion cause the deposition. The role of thermophoresis on the particle deposition was then assessed from the difference between depositions with and without the temperature gradient.

Experimental matrix

We used gold, silver, and palladium electrodes with diameters of 1.63, 2.06, and 1.63 mm (Surepure Chemetals), respectively, to generate the nanoparticles. Particles were deposited on TEM grids for 2 min time periods under both isothermal and thermophoretic conditions at spark frequencies of 3, 9, 15, and 30 Hz for each material. Size distributions were measured for aerosol (particle laden gas) entering and exiting deposition cell in all cases. The effluent from the thermophoretic particle deposition cell was passed through a series of high efficiency particulate air (HEPA) filters (TSI Inc.) to remove any remaining particles.

Characterization

We characterized the deposited particles for their shape and size with a TEM (JEM-1400, JEOL Ltd.). Size distribution measurements for the aerosol were obtained with an SMPS (Model 3936, TSI) spectrometer. It consists of an Electrostatic Classifier (Model 3080L, TSI) and an ultrafine condensation particle counter (UCPC) (Model 3776, TSI). The SMPS spectrometer measures the size distribution of submicrometer aerosols using a technique based on differences in the mobility of charged particles in an electrical field. Particles entering the SMPS system are neutralized using a radioactive source so that they exhibit a Fuchs equilibrium charge distribution. They then enter the electrostatic classifier where particles are classified according to their electrical mobilities when the particles in a narrow mobility window exit through an output slit to be counted. This narrow distribution is then directed to the UCPC which determines the particle concentration in that mobility window.

Experimental results and discussions

SMPS measurements

Scanning mobility particle sizer size distribution measurements were obtained for two different deposition cases: isothermal and thermophoretic deposition. In both cases, size distributions were obtained for spark frequencies of 3, 9, 15, and 30 Hz. Here, we have not reported the size distributions for particles directly exiting the particle generator, since the difference between such direct measurements and the distributions downstream of deposition cell (isothermal deposition) was observed to be negligible.

Results for gold, silver, and palladium particles are shown in Figs. 2, 3, and 4, respectively. The particle concentration peaks increase in magnitude and area with increasing spark frequency and the peaks also shift towards larger particle diameters in all cases. The peak (most probable) diameters are listed in Table 1.

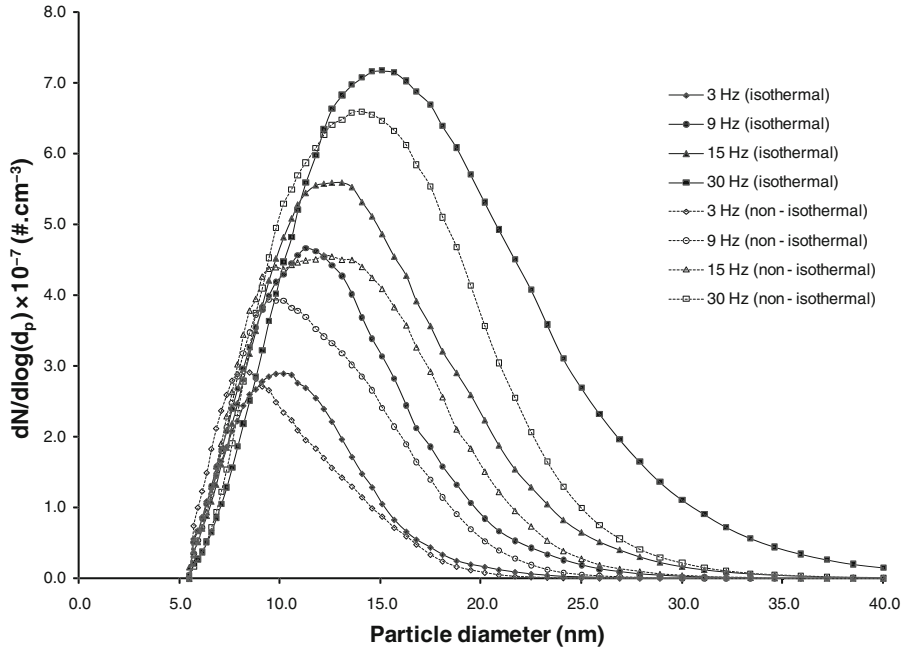

Fig. 2 Gold nanoparticle size distributions, for spark frequencies of 3, 9, 15, and 30 Hz. *Solid symbols* are used for the data from isothermal deposition cases and *hollow symbols* are used for thermophoretic deposition cases

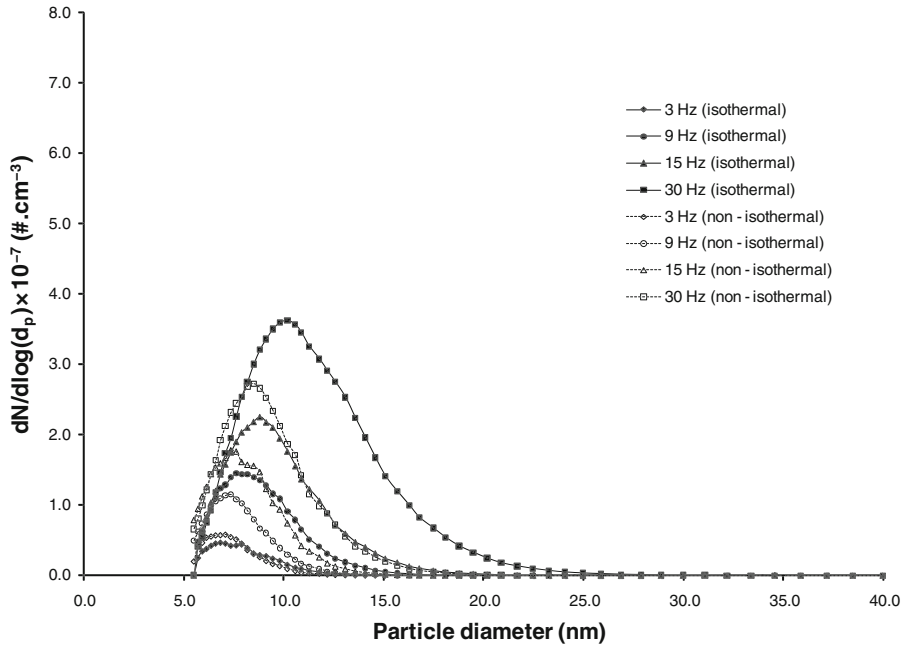

Fig. 3 Silver nanoparticle size distributions, for spark frequencies of 3, 9, 15, and 30 Hz. *Solid symbols* are used for the data from isothermal deposition cases and *hollow symbols* are used for thermophoretic deposition cases

Figure 5 shows the cumulative mass concentration plot for the gold nanoparticles measured downstream of the deposition cell with and without thermophoretic deposition. The differences in the cumulative mass concentrations of the particles generated with and without the thermophoretic deposition give estimates of the thermophoretic deposition fractions in the deposition cell. For silver and palladium nanoparticles, similar cumulative mass concentration trends were observed.

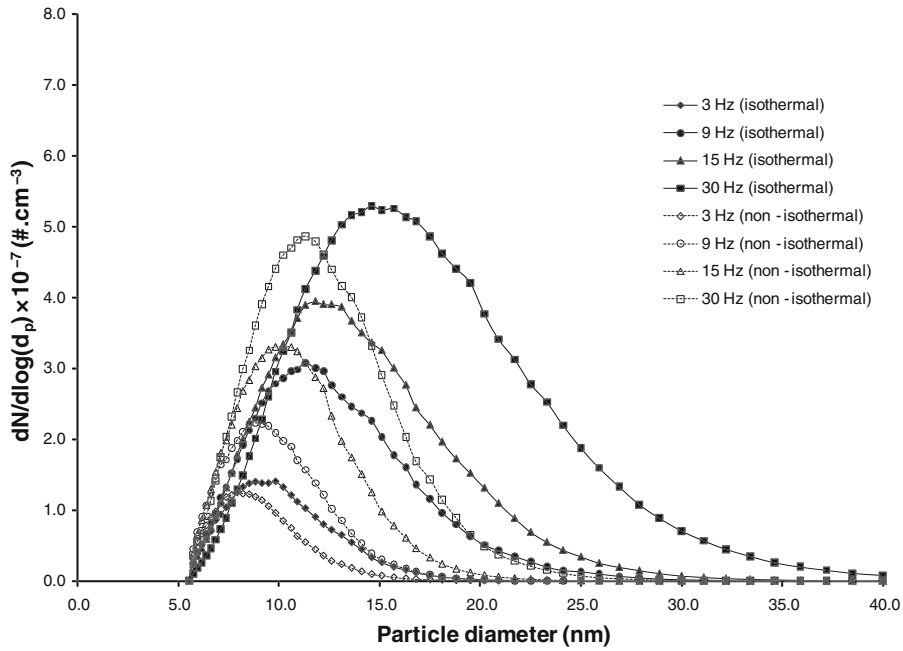

Fig. 4 Palladium nanoparticle size distributions, for spark frequencies of 3, 9, 15, and 30 Hz. *Solid symbols* are used for the data from isothermal deposition cases and *hollow symbols* are used for thermophoretic deposition cases

Table 1 Diameters at which the size distribution peaks for observed for gold, silver, and palladium nanoparticles generated at spark frequencies 3, 9, 15, and 30 Hz

Spark frequency (Hz)	Size distribution peak diameters (nm)		
	Gold	Silver	Palladium
3	10.2	7.91	9.82
9	11.3	8.2	11.3
15	13.1	8.82	11.8
30	15.1	10.2	14.6

Particle deposition increased in all cases with increasing spark frequency because of the higher generation rate of particles. The rate of particle generation (evaporation rate) is dependent on the energy input, and the higher the frequency, the higher is the energy input. Our tests on the GFG-1000 show a linear dependence of the particle mass production rate on the spark frequency as was previously reported by Tabrizi et al. (2009) and Boddu et al. (2011). This clearly provides a mechanism by which the particle mass production rate can be conveniently controlled although one must note that the particle size distribution both widens and shifts up with increasing spark frequency which is indicative of either increased particle agglomeration, increased condensation, or both, as the amount of evaporated material increases with spark frequency.

TEM characterization

Figure 6 shows TEM images of gold and silver nanoparticles and palladium nanoparticles/nano-agglomerates that were collected on TEM grids. The gold nanoparticle shown in Fig. 6a is a single particle selected randomly from the multiple particles. It has a crystalline structure which is very typical of gold nanoparticles generated by the spark generation method (Tabrizi et. al. 2009). The silver particle (Fig. 6b) is more spherical and it is also smaller in size as compared with the gold particles. As shown in Fig. 6c1 and c2, for palladium both nanoparticles and nano-agglomerates were produced. Thermal conductivity of the material influences the particle formation, its size, and also its agglomeration to a certain extent. Thermal conductivities of gold, silver, and palladium are 318, 429, and 71.8 W m^{-1} K^{-1}. The thermal conductivity of palladium is significantly lower than both gold and silver, which allows palladium nanoparticles to remain active (hotter) for relatively longer period of time, possibly enhancing more interaction

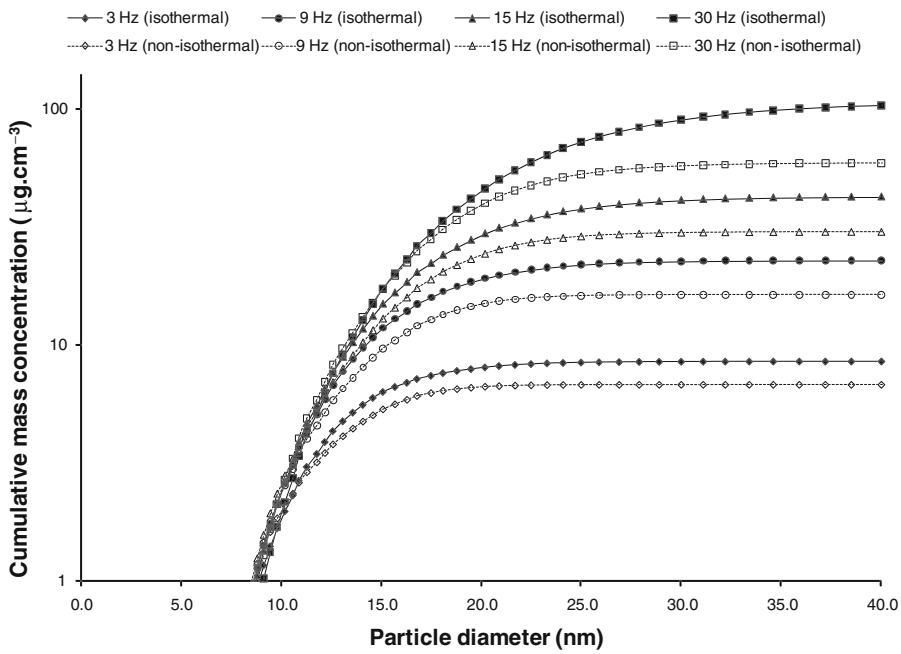

Fig. 5 Gold nanoparticles cumulative mass concentration curves versus particle diameter. *Solid symbols* are used for the data from isothermal deposition cases and *hollow symbols* are used for thermophoretic deposition cases

among particles, leading to further agglomeration. However, the size of the agglomerated palladium particles was still below 50 nm, and the diameter of individual particles was less than 10 nm.

Figure 7 shows the images of nanoparticles deposited on TEM grids that were generated at a spark frequency of 30 Hz, but were collected by two different methods: diffusion and thermophoresis. The increase in particle deposition due to thermophoresis was evident from these TEM micrographs. Similar results were obtained for particles generated at spark frequencies of 3, 9, and 15 Hz. The SMPS measurements correlated well with the deposition densities observed in the corresponding TEM images. Visually, the impact of the thermophoresis on the collection efficiency is readily apparent as increased deposition in every case.

Figure 8 shows the SEM images of randomly selected gold, silver, and palladium single particles and their corresponding EDS spectrum for the particle. For EDS analysis, relatively larger size particles were chosen for better resolution of the EDS spectrum. The EDS analysis showed the particles to be extremely pure. The C-peak was due to the carbon film substrate on the TEM grid (carbon-coated copper grid). The gold, silver, and palladium single nanoparticles (shown in Fig. 8) are spherical with the diameters of 1, 1.1, and 1.53 μm, respectively. This, together with the TEM images of palladium nano-agglomerates, suggests that while agglomeration was dominant in the formation of palladium particles, a few particles grew by condensation alone.

CFD model for the transport and deposition of nanoparticles

A CFD simulation that maintains good fidelity with the experimental system is difficult to achieve because of the complexities associated with a source reinforced aerosol that is charged and which is subject to both condensation and agglomeration. We have, therefore, used the CFD code Fluent (Ansys) to compute theoretic deposition mass fractions for gold, silver, and palladium nanoparticles in our deposition cell, albeit subject to necessary simplifying assumptions. Specifically, we have neglected the source reinforcement, condensation, coagulation, and charge effects. In our particle deposition model however, the convective, diffusive, and thermophoretic forces acting on the particles are all considered. The detailed particle deposition model was adopted from Gutti and Loyalka (2009). We assume that a fully developed flow of argon gas with entrained particles entered the deposition cell with a flow rate of 5 L min^{-1} at a temperature of 100 °C for the thermophoretic

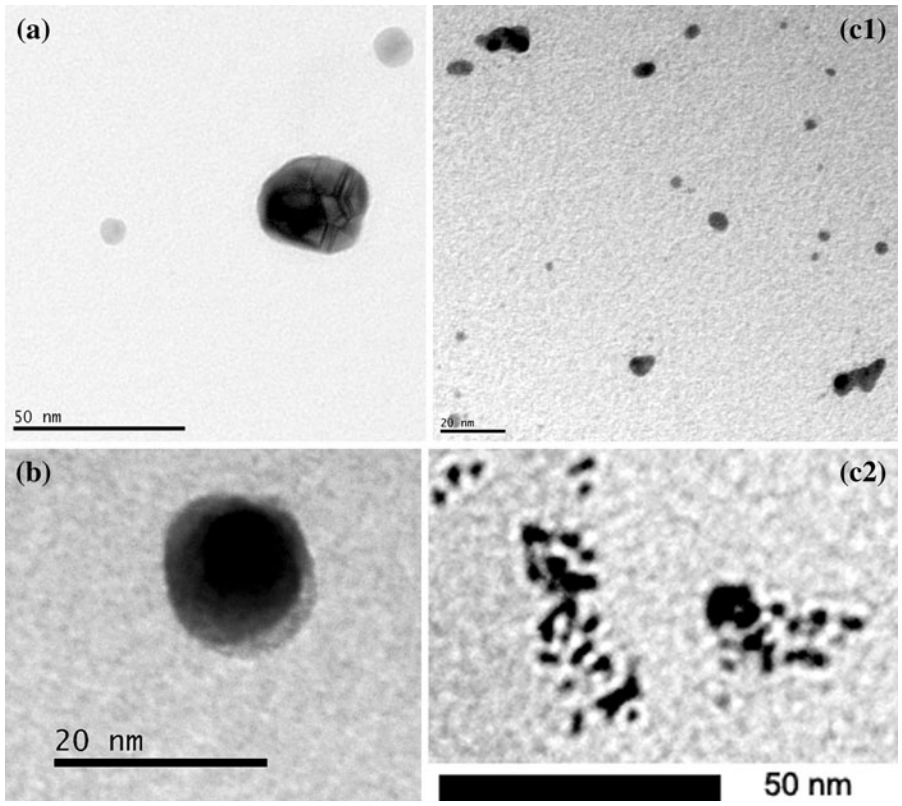

Fig. 6 **a** TEM image of a ~25 nm gold nanoparticle (*scale size* 50 nm). **b** TEM image of a ~15 nm silver nanoparticle (*scale size* 20 nm). **c1** TEM image of palladium nanoparticles/nano-agglomerates of size $\lesssim$ 15 nm (*scale size* 20 nm). **c2** TEM image of palladium nano-agglomerates

deposition case and at room temperature (25 °C) for the isothermal deposition case. The flow conditions used are taken from the actual particle deposition experiments that were run and are summarized in Table 2 along with other parameters used in the computations. The discrete phase model (DPM) within Fluent was employed to track the particle flow path and deposition in the deposition cell and a thermophoretic force term acting on the particle was used (Boddu et al. 2011).

We employed a fine mesh with 5,919,204 total compute volumes and a 16-processor computer cluster to compute the deposition efficiencies for both the isothermal and thermophoretic cases (the deposition efficiency is defined as the fraction of the particles at the inlet deposited on the TEM grid). Deposition efficiencies calculated for particle sizes of 50, 100, 200, and 300 nm for both the cases are shown in Table 3. The deposition efficiencies increased with particle diameter for all materials. Further, deposition efficiencies for isothermal cases were observed to be similar (with very small differences) among the three materials investigated for a given particle diameter. However, deposition efficiencies increased in thermophoretic cases for a given particle diameter, in the order silver < gold < palladium for all diameters with one exception in our results for 300 nm particles, where the order was gold < silver < palladium.

Particle deposition in thermophoretic case is influenced by the thermal properties of the material. As particle thermal conductivity increases, the expectation is that the thermophoretic force on the particle decreases (Fernandes and Loyalka 1996; Brock 1962; Loyalka 1992; Li and Davis 1995). Since the thermal conductivity of silver is greater than that of either gold or palladium, silver particles should experience smaller thermophoretic forces which could lead to deposition of fewer particles on the collection grids than for either gold or palladium (keeping all other parameters constant). Both our data and computational

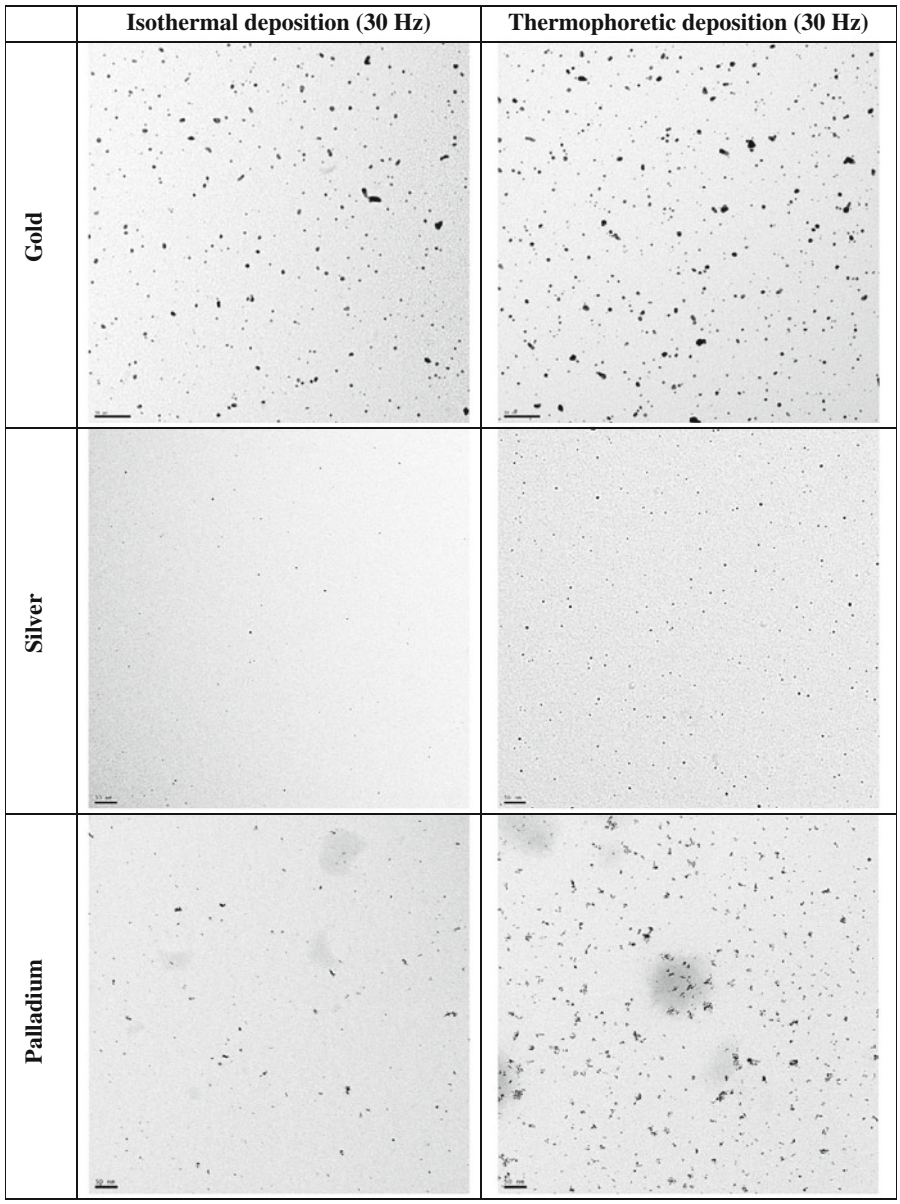

Fig. 7 TEM images of deposited gold, silver, and palladium nanoparticles for isothermal and thermophoretic deposition cases at spark frequency of 30 Hz. All images are at indicated magnification of 25,000× and the *scale size* on the images are 50 nm (0.05 μm)

results are consistent with this prediction (Fig. 8; Table 3).

Conclusions

We have explored gold, silver, and palladium nanoparticle generation, collection, and characterization. We have found that the nanoparticle mass production rate and size distribution peak diameter can be controlled by changing the sparking frequency in the spark aerosol generator. We have also found that the particle collection on TEM grids is enhanced by thermophoresis in all the cases we have studied. The CFD results are consistent with the data.

The TEM images of the collected particles show them to be predominantly single particles for gold and silver, and nano-agglomerates for palladium. The SEM images show that some large particles in the micron range were also produced, but they were very spherical (for gold, silver, and palladium) indicating that they grew as single particles by condensation

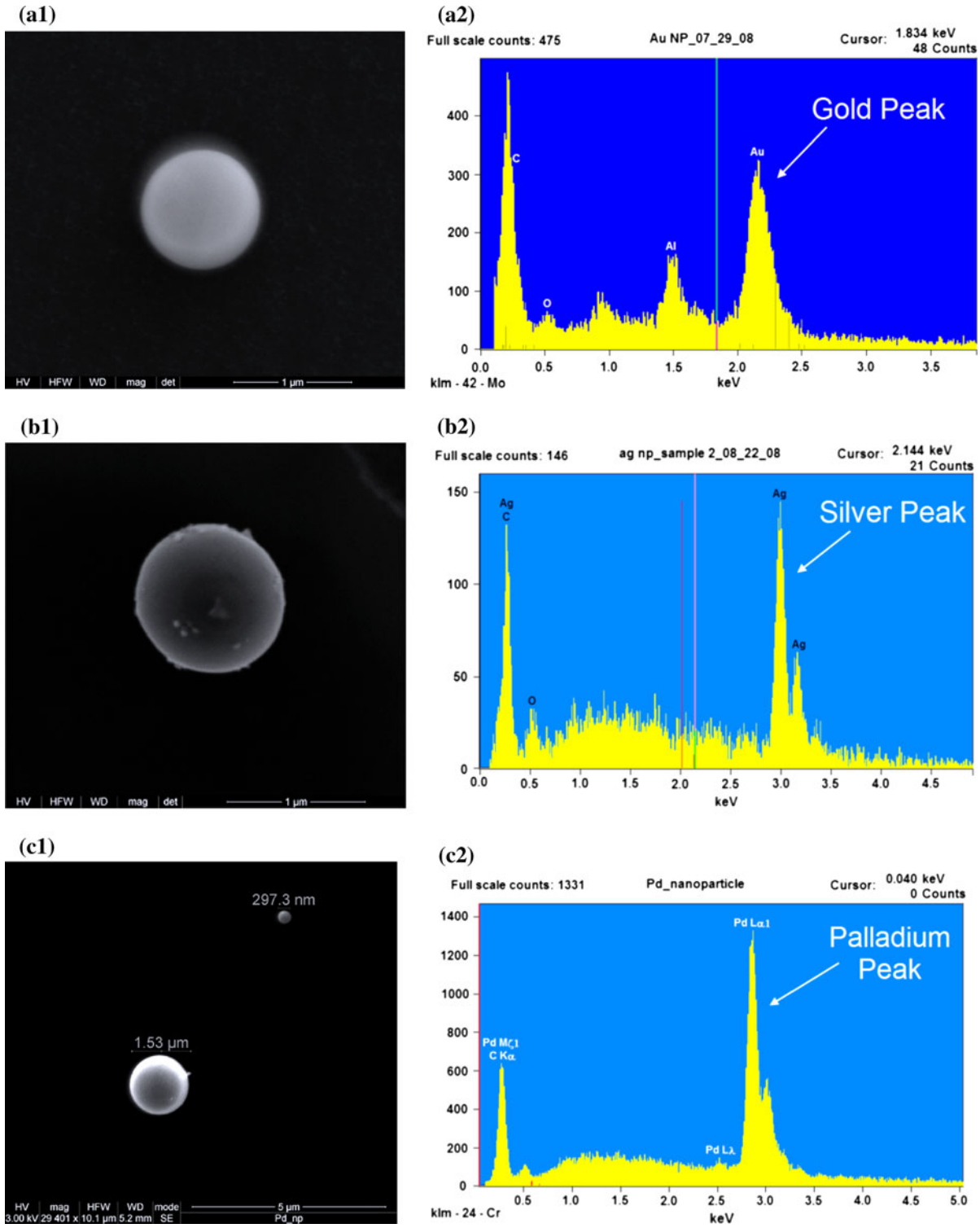

Fig. 8 SEM images of some larger nanoparticles **a1** gold, **b1** silver, and **c1** palladium. Energy dispersive X-ray spectra (EDS) of the particles **a2** gold, **b2** silver, and **c2** palladium, confirms the particles for gold, silver, and palladium, respectively

Table 2 Input values for the Fluent CFD computational model

Inlet gas temperature	100 °C (thermophoretic)
	25 °C (isothermal)
Deposition surface temperature	7 °C (thermophoretic)
	25 °C (isothermal)
Inlet flow velocity magnitude	4.67 m s^{-1}
Particle inlet flow velocity magnitude	4.67 m s^{-1}
Inlet particle temperature	100 °C (thermophoretic)
	25 °C (isothermal)
Particle sizes modeled	50, 100, 200, and 300 nm
Particle mass flow rates modeled	1×10^{-7} kg s^{-1} for (50 and 100 nm)
	5×10^{-7} kg s^{-1} for (200 and 300 nm)

Table 3 Predicted deposition efficiencies for gold, silver, and palladium nanoparticles of various sizes calculated from the CFD computations of particle deposition in the deposition cell for the isothermal (I) and thermophoretic (II) cases

Particle size (nm)	Deposition efficiency (mass fraction)					
	Gold		Silver		Palladium	
	I	II	I	II	I	II
50	0.006	0.027	0.008	0.021	0.010	0.0318
100	0.011	0.042	0.009	0.032	0.016	0.0637
200	0.012	0.064	0.018	0.053	0.021	0.0806
300	0.017	0.074	0.018	0.085	0.022	0.0955

alone. This holds the possibility that by optimally controlling the argon flow rate and the spark frequency, one could control both the agglomeration and the condensational growth, and produce particles in a narrow and well defined range.

We note that the basic concepts employed in this study for the collection of samples and for the computational analysis of the particle deposition can also be used to study the fundamental transport and deposition properties of many other different particles, including those with complex shapes, or incorporating radioactivity, or charge on many different types of surfaces. For example, radioactive gold nanoparticles could be used for the study of the influence of radioactivity on particle deposition and/or growth by condensation and agglomeration.

Acknowledgments This research has been supported by the following grants from the Department of Energy: Nuclear Energy Research Initiative (NERI-C; Grant # DE-FG07-07ID14892), Innovations in Nuclear Education and Infrastructure (INIE; Grant # DE-FG07-03ID14531), and Global Nuclear Energy Partnership (GNEP; grant DE-FG07-07ID14851).

References

Ache HJ, Baetsle LH, Bust RP, Nechaev AF, Popik VP, Ying Y (1989) Feasibility of separation and utilization of ruthenium, rhodium and palladium from high level waste. IAEA, technical report series No. 308, Vienna

Antonello DP, Bocci G (2007) Drug distribution in tumors: mechanisms, role in drug resistance, and methods for modification. Curr Onco Rep 9:109–114

Bae CH, Nam SH, Park SM (2002) Formation of silver nanoparticles by laser ablation of a silver target in NaCl solution. Appl Surf Sci 197–198:628–634

Boddu S, Gutti VR, Meyer RM, Tompson RV, Loyalka SK (2011) Carbon nanoparticle generation, collection, and characterization using a spark generator and a thermophoretic deposition cell. Nucl Technol (in publication)

Brock JR (1962) On the theory of thermal forces acting on aerosol particles. J Colloid Sci 17(8):768–780

Byeon JH, Park JH, Hwang J (2008) Spark generation of monometallic and bimetallic aerosol nanoparticles. J Aerosol Sci 39:888–896

Cao G (2004) Nanostructures and nanomaterials: synthesis, properties, and applications. Imperial College Press, London

Chaudhari VR, Harama SK, Kulshreshtha SK, Bellare JR, Hassan PA (2007) Synthesis of silver nanoparticles by chemical reduction method and their antibacterial activity. Colloids Surf A Physicochem Eng Asp 301:475–480

Chen Z, Gao L (2007) A facile and novel way for the synthesis of nearly monodisperse silver nanoparticles. Mater Res Bull 42:1657–1661

De Jong WH, Hagens WI, Krystek P, Burger MC, Sips AJAM, Geertsma RE (2008) Particle size-dependent organ distribution of gold nanoparticles after intravenous administration. Biomaterials 29:1912–1919

Evans DE, Harrison RM, Ayres JG (2003) The generation and characterization of metallic and mixed element aerosols for human challenge studies. Aerosol Sci Technol 37:975–987

Fernandes A, Loyalka SK (1996) Modeling of thermophoretic aerosol deposition in nuclear reactor containments. Nucl Technol 116(3):270–282

Frieboes HB, Sinek JP, Nalcioglu O, Fruehauf JP, Cristini V (2006) Nanotechnology in cancer drug therapy: a biocomputational approach. In: BioMEMS and Biomedical Nanotechnology, Vol 1. Springer, New York

Giridhar P, Venkatesan KA, Reddy BP, Srinivasan TG, Rao PRV (2006) Recovery of fission palladium by electrodeposition using room temperature ionic liquids. Radiochim Acta 94:131–136

Gutti VR, Loyalka SK (2009) Thermophoretic deposition in a cylindrical tube: computations and comparison with experiments. Nucl Technol 166(2):121–133

Hsu H (2004) Photochemical synthesis of gold nanoparticles with interesting shapes. NNIN REU Research accomplishments:68–69

Huang X (2006) Gold nanoparticles used in cancer cell diagnostics, selective photothermal therapy and catalysis of NADH oxidation reaction. Dissertation, Georgia Institute of Technology, Atlanta

Jenson GA, Rohmann CA, Perrigo LD (1980) Recovery and use of fission product noble metals. Transactions ANS 34: 335–336

Kannan R, Rahing V, Cutler C, Pandrapragada R, Katti KK, Kattumuri V, Robertson JD, Casteel SJ, Jurisson S, Smith C, Boote E, Katti KV (2006) Nanocompatible chemistry toward fabrication of target-specific gold nanoparticles. J Am Chem Soc 128:11342–11343

Kim YH, Lee DK, Kang YS (2005) Synthesis and characterization of Ag and Ag-SiO2 nanoparticles. Colloids Surf A Physicochem Eng Asp 257–258:273–276

Kumar A, Joshi H, Pasricha R, Mandale AB, Sastry M (2003) Phase transfer of silver nanoparticles from aqueous to organic solutions using fatty amine molecules. J Colloid Interface Sci 264:396–401

Lehtinen KEJ, Backman U, Jokiniemi JK, Kulmala M (2004) Three-body collisions as a particle formation mechanism in silver nanoparticle synthesis. J Colloid Interface Sci 274: 526–530

Li W, Davis EJ (1995) The effects of gas and particle properties on thermophoresis. J Aerosol Sci 26:1085–1099

Loyalka SK (1992) Thermophoretic force on a single particle-I. Numerical solution of the linearized Boltzmann equation. J Aerosol Sci 23(3):291

Ozawa M, Shinoda Y, Sano Y (2002) The separation of fission product rare elements toward bridging the nuclear and soft energy systems. Prog Nucl Energ 40:527–538

Pal A, Shah S, Devi S (2007) Synthesis of Au, Ag and Au-Ag alloy nanoparticles in aqueous polymer solution. Colloids Surf A Physicochem Eng Asp 302:51–57

Patel K, Kapoor S, Dave DP, Mukherjee T (2005) Synthesis of Pt, Pd, Pt/Ag and Pd/Ag nanoparticles by microwave-polyol method. J Chem Sci 117(4):311–315

Pathak P, Katiyar VK, Giri S (2007) Cancer research-nanoparticles, nanobiosensors and their use in cancer research. J Nanotechnol. doi: 10.2240/azojono0116

Tabrizi NS, Ullmann M, Vons VA, Lafont U, Schmidt-Ott A (2009) Generation of nanoparticles by spark discharge. J Nanopart Res 11:315–332

Zhang JP, Chen P, Sun CH, Hu X (2004) Sonochemical synthesis of colloidal silver catalysts for reduction of complexing silver in DTR system. Appl Catal A 266:49–54